New Robust Luminescent Supramolecular Assemblies Based on [Ln(Mo 8 O 26) 2] 5– (Ln = Eu, Sm) Polyoxometalates

Patricia Bolle, Nicolas Albrecht, Thibault Amiaud, Bernard Humbert, Eric Faulques, Remi Dessapt, Hélène Serier-Brault

New robust luminescent supramolecular assemblies based on $[Ln(Mo_8O_{26})_2]^{5-}$ (Ln = Eu and Sm) polyoxometalates

Patricia Bolle, Nicolas Albrecht, Thibault Amiaud, Bernard Humbert, Eric Faulques, Rémi Dessapt,* Hélène Serier-Brault*

Institut des Matériaux Jean Rouxel (IMN), Université de Nantes, CNRS, 2 rue de la Houssinière, BP 32229, 44322 Nantes cedex 3, France

Supporting Information Placeholder

ABSTRACT: This work highlights for the first time the photoluminescence (PL) properties of two new $[Ln(Mo_8O_{26})_2]^{5-}$ (Ln = Eu, Sm) lanthanide-containing polyoxometalates. Stable crystals of the tetrabutylammonium salts $(TBA)_5[Ln(Mo_8O_{26})_2]$ were synthesized, and their structures were confirmed by single-crystal X-ray diffraction. The robustness of the $[Ln(Mo_8O_{26})_2]^{5-}$ complexes in acetonitrile solution has been evidenced by FT-Raman and PL spectroscopies. Then, the tetraphenylphosphonium $(TPP)_5[Ln(Mo_8O_{26})_2]$ derivatives were obtained by a salt metathesis reaction. The two series exhibit a high thermal stability in air and are efficient solid-state phosphors at room temperature.

Polyoxometalates incorporating Ln^{3+} lanthanide ions (Ln-POMs) form a fascinating class of nanosized metal-oxide clusters of early transition metals (M = Mo, W, V).[1] They are currently the focus of intense researches owing to their promising applications in the fields of single molecule magnets (SMMs),[2] catalysis,[3] and especially photoluminescence (PL).[4] $Na_9[EuW_{10}O_{36}]\cdot xH_2O$ (**EuW_{10}**) has been extensively investigated due to its remarkable PL properties[5] which were recently used to elaborate chemical probes for biology,[6] photocatalysts[7] and luminescent thermometers.[8] In the Weakley-type $[Eu(W_5O_{18})_2]^{9-}$ complex, the POM ligands act as sensitizers to exalt the luminescence of the Eu^{3+} ion via an antenna effect.[5] $[Eu(W_5O_{18})_2]^{9-}$ has been also ionically incorporated into organic polymers,[9] vesicles,[10] surfactants,[11] ionic liquids,[12] and metal-organic frameworks[8] to design hybrid organic-inorganic photoactive composites. However, because of its huge negative charge and the insolubility of **EuW_{10}** in most of non-aqueous solutions, the assembly of $[Eu(W_5O_{18})_2]^{9-}$ with organic cations into crystallized supramolecular frameworks is more critical and was very rarely reported.[13] Other Eu-POMs were since designed,[4c,5,14] but they are less efficient emitters than **EuW_{10}** because i) they contain corner-shared MO_6 octahedra that favor the electron-to-hole recombination into the POM ligands instead of POM-to-Eu^{3+} energy transfers, ii) the Ln^{3+} ions are too close to each other leading to PL concentration quenching effects or iii) water molecules link the Eu^{3+} ions and promote non-radiative deactivation from its $^5D_0$ emitting level.[15] In addition, most of these compounds are hydrated alkali salts which exhibit a limited thermal stability. Thus, the discovery of Ln-POMs with lower charges, and soluble in non-aqueous solvents is still highly challenging. In 1997, Kitamura *et al.* reported tetrabutylammonium (TBA) salts of the $[Ln(Mo_8O_{26})_2]^{5-}$ complex (Ln = La, Y, Ce Pr, Nd, Gd, Yb) (Figure 1a).[16] Other Ln-derivatives (Tb, Dy, Ho, Er, Tm) were recently obtained which exhibit interesting SMM properties.[17] However, crystals of these efflorescent acetonitrile solvates degrade rapidly in air, leading to structurally uncharacterized powders. In addition, the photophysical properties of these Ln-POMs have never been investigated, and their Eu and Sm counterparts have not been designed yet.

We report herein the synthesis and structural characterization of two new thermally robust $(TBA)_5[Ln(Mo_8O_{26})_2]$ compounds (**TBA-$EuMo_{16}$** and **TBA-$SmMo_{16}$**), and their Y^{3+}-counterpart (**TBA-YMo_{16}**). Their tetraphenylphosphonium (TPP) derivatives $(TPP)_5[Ln(Mo_8O_{26})_2]$ (**TPP-$LnMo_{16}$**) were also prepared in acetonitrile by a salt metathesis reaction. The photophysical properties of these phosphors were thoroughly investigated and discussed.

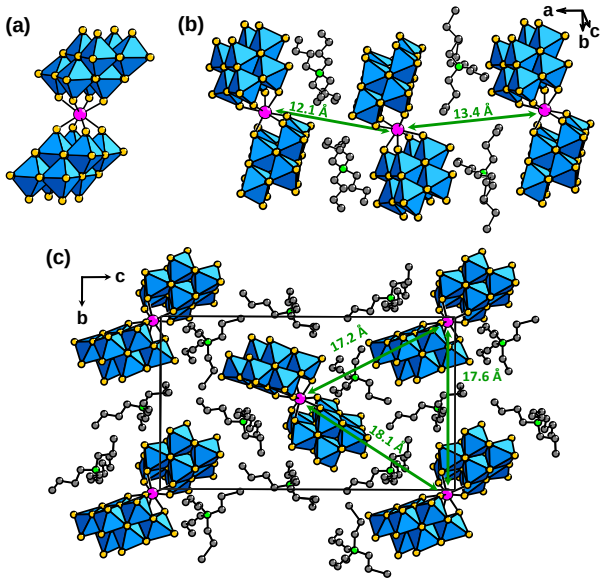

Figure 1. a) Structure of the $[Eu(Mo_8O_{26})_2]^{5-}$ complex. b) Supramolecular $\{(TBA)_2[Eu(Mo_8O_{26})_2]\}^{3-}$ ribbon. c) Crystal packing in **TBA-$EuMo_{16}$**. Green arrows indicate the Eu···Eu distances (blue octahedra = MoO_6, gold sphere: oxygen, pink sphere: europium, green sphere: nitrogen, grey sphere: carbon. H-atoms are omitted).

The syntheses of the six compounds are described in the Supporting Information. The TBA-$LnMo_{16}$ systems were obtained as colorless crystals by slightly modifying the synthesis route developed for other Ln-derivatives.[17] Our synthetic procedure also differs from that previously reported for **TBA-YMo_{16}**.[16] FT-IR spectroscopy (Figure S1), TGA measurements (Figure S2) along with elemental analyses confirm the chemical composition

$(TBA)_5[Ln(Mo_8O_{26})_2]$. Noticeably, crystals are stable in air, and no efflorescence appears even after several months. Powder X-Ray diffraction (PXRD) analysis shows that the three compounds are isostructural (Figure S3). The structures of **TBA-EuMo$_{16}$** and **TBA-SmMo$_{16}$** were resolved by single-crystal X-ray diffraction (Table S1), and that of **TBA-EuMo$_{16}$** is described below. In $[Eu(Mo_8O_{26})_2]^{5-}$, two β-$[Mo_8O_{26}]^{4-}$ units connect a central Eu^{3+} ion (Figure 1a) which is located into a distorted square antiprismatic site. Supramolecular $\{(TBA)_2[Eu(Mo_8O_{26})_2]\}^{3-}$ ribbons run along the *a* axis (Figure 1b) with long intermolecular Eu···Eu distances of 12.1 Å and 13.4 Å. Ribbons are separated by TBA units (Figure 1c) with the shortest inter-ribbon Eu···Eu distance of 17.2 Å. As suspected, the structures do not show any crystallized acetonitrile molecules. This is consistent with the absence in the Raman spectra of the intense ν(C≡N) stretching mode around 2260 cm^{-1} (Figure S4).[18] In addition, TGA measurements (Figure S2) confirm the stability of compounds in air up to 275°C.

FT-Raman spectroscopy is a powerful tool to characterize POMs in solution and in the solid state.[19] Figure S5 displays the Raman spectra of **TBA-EuMo$_{16}$** in acetonitrile solutions at three concentrations i.e., 2 .10^{-2} M, 10^{-2} M, and 5 .10^{-3} M. In the 150-1000 cm^{-1} range, the Raman peaks characteristic of $[Eu(Mo_8O_{26})_2]^{5-}$ match with those recorded for the **TBA-EuMo$_{16}$** solid phase. In this concentration range, no additional signals that could indicate its partial degradation are observed. Moreover, the intensity of the main line at 977 cm^{-1} attributed to the terminal Mo=O bonds increases linearly with the Eu-POM concentration (Figure S6). In addition, a statistical analysis by "separation curve method" reveals that the spectra recorded in solution are perfectly similar to the solid one. This quantitatively confirms the integrity of the Ln-POM complex in solution. Then, by exchanging TBA cations by TPP ones, **TPP-LnMo$_{16}$** (Ln = Eu, Sm) and their Y^{3+} counterpart were prepared as microcrystalline powders. Attempts to isolate single-crystals were unsuccessful. However, PXRD analyses show that they are isostructural (Figure S3). Finally, FT-IR (Figure S1) and FT-Raman (Figure S7) spectroscopies, elemental analyses, and TGA measurements (Figure S2) indicate a TPP:Ln-POM ratio of 5 : 1, and show that the compounds are thermally stable in air up to 355°C.

The solid-state absorption spectra of the TBA-$LnMo_{16}$ series (Figure S8) show two broad bands at 270 and 305 nm, which are assigned to mixed O→Mo and O→Eu ligand-to-metal charge-transfer (LMCT) transitions. Similar bands are observed for the TPP-$LnMo_{16}$ series, with a more intense transition at 270 nm, because the cation absorbs at this wavelength. The six compounds have an optical band gap of 370 nm. In addition, room-temperature time-resolved PL spectroscopy has been performed to characterize the intrinsic luminescence of the POM ligands. Upon photoexcitation into the O→Mo LMCT band, the Ln-free reference **TBA-YMo$_{16}$** shows a broad emission band centered at 385 nm (Figure S9) with a short mean luminescence lifetime of τ = 0.382 μs (Table S2). This band can be decomposed into two contributions at 364 (27473 cm^{-1}) and 418 nm (23923 cm^{-1}) (Table S2). Comparable emissions are also observed for the TBA-$LnMo_{16}$ (Ln = Eu, Sm) compounds and their TPP counterparts (Figure S9), with similar decay times (Table S2). Based on earlier studies,[1c,4c] these bands have been assigned to the $^3T_{1u}\rightarrow{}^1A_{1g}$ transitions originating from the two O→Mo LMCT emitting triplet states of the POM ligands.

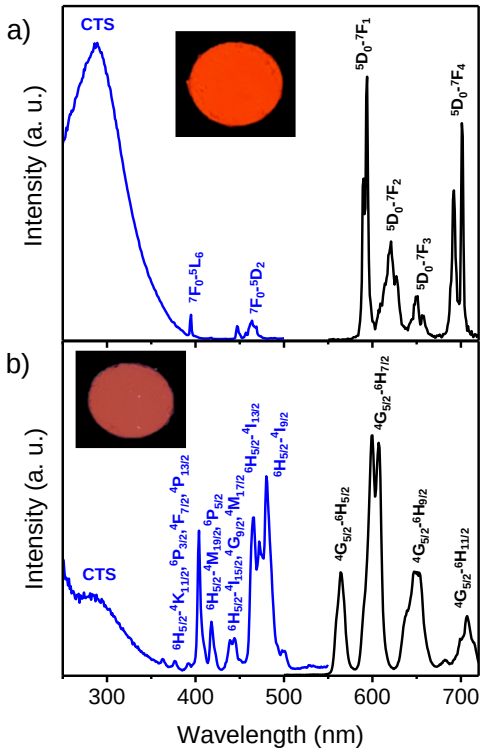

Figure 2. a) Excitation spectrum (blue line) monitored at 594 nm and emission spectrum (black line) monitored at 286 nm of **TBA-EuMo$_{16}$**. Inset: Photograph of the powder of **TBA-EuMo$_{16}$** upon irradiation at 254 nm. b) Excitation spectrum (blue line) monitored at 600 nm and emission spectrum (black line) monitored at 286 nm of **TBA-SmMo$_{16}$**. Inset: Photograph of the powder of **TBA-SmMo$_{16}$** upon irradiation at 254 nm.

The room-temperature steady-state photoluminescence excitation (PLE) and emission spectra of **TBA-EuMo$_{16}$** and **TBA-SmMo$_{16}$** are depicted in Figure 2. Upon irradiation at 254 nm with a standard UV lamp, **TBA-EuMo$_{16}$** exhibits a strong orange-red emission (Figure 2a). Its PLE spectrum monitored at 594 nm shows a broad intense band at 286 nm (34965 cm^{-1}) which corresponds to the charge-transfer states (CTS), mainly dominated by the $^1A_{1g}\rightarrow{}^1T_{1u}$ transition of the O→Mo LMCT photoexcitation.[4c] Several sharp lines are also observed which are characteristic of the intra-configurational f-f transitions of Eu^{3+} *i.e.*, $^7F_0\rightarrow{}^5L_6$ (395 nm) and $^7F_0\rightarrow{}^5D_2$ (464 nm). Noticeably, the f-f transitions got a very weak intensity which indicates that the most efficient excitation process corresponds to the CTS. Thus, the β-$[Mo_8O_{26}]^{4-}$ ligands are effective light-harvesting antennae to sensitize the Eu^{3+} ion through an intramolecular energy transfer from the $^3T_{1u}$ excited levels to the emitting $^5D_0$ level, lying at a lower energy (Figure S10). Upon photoexcitation into the CTS band, the PL spectrum of **TBA-EuMo$_{16}$** consists in a multi-band emission characteristic of the $^5D_0\rightarrow{}^7F_J$ (J = 0-4) transitions of an Eu^{3+} ion occupying an asymmetric site with approximate D_{4d} symmetry.[20] Indeed, the symmetry-forbidden $^5D_0\rightarrow{}^7F_0$ electric-dipole transition is absent. The strongest $^5D_0\rightarrow{}^7F_1$ magnetic-dipole transition is split into two Stark components at

590 and 594 nm. The $^5D_0 \rightarrow {}^7F_2$ electric-dipole transition (611-630 nm), which is highly sensitive to the chemical surrounding at the vicinity of Eu^{3+} and the $^5D_0 \rightarrow {}^7F_3$ transition (648-661 nm) got weak intensities. In contrast, the $^5D_0 \rightarrow {}^7F_4$ split-band (692 and 701 nm) is intense. Thus, the emission of **TBA-EuMo$_{16}$** is characterized by CIE chromaticity coordinates of (0.6255, 0.3681) (Figure S11). The $^5D_0 \rightarrow {}^7F_1$ transition exhibits a long luminescence lifetime of 5.24 ± 0.03 ms (Figure S12). Noticeably, the emission spectrum of **TBA-EuMo$_{16}$** shows the same feature than that of **EuW$_{10}$** and their PL performances are close.[5] This can be explained considering that $[Eu(Mo_8O_{26})_2]^{5-}$ and $[Eu(W_5O_{18})_2]^{9-}$ have some structural similarities. Indeed, they contain POM ligands only built upon edge-shared MO_6 octahedra that discriminates against thermally activated hopping of d^1 electrons and limits the M→O non-radiative deactivation processes.[22,4c] They also exhibit low average M-O-Eu bond angle values (131.3° and 130.17° for **TBA-EuMo$_{16}$** and **EuW$_{10}$**,[21] respectively). This contributes to prevent the PL quenching of Eu^{3+} due to d^1 electron hopping through fπ-pπ-dπ orbital mixing, which is rather favored for higher bond angle values.[4b,c] Moreover, the Eu^{3+} ion occupies a similar distorted square antiprismatic site without coordinated water molecules likely to quench its luminescence.[22] Finally, the long Eu···Eu distances, higher than 12 Å, may suggest that side PL concentration quenching effects should be strongly minimized. The orange emission of **TBA-SmMo$_{16}$** at room temperature is less intense than that of **TBA-EuMo$_{16}$** (Figure 2b). The PLE spectrum contains the CTS band (286 nm) and sharp lines associated to the f-f transitions of Sm^{3+}, *i.e.* $^6H_{5/2} \rightarrow {}^4K_{11/2}$, $^6P_{3/2}$, $^4F_{7/2}$, $^4P_{13/2}$ (404 nm), $^6H_{5/2} \rightarrow {}^4M_{19/2}$, $^6P_{5/2}$ (418 nm), $^6H_{5/2} \rightarrow {}^4I_{15/2}$, $^4G_{9/2}$, $^4M_{17/2}$ (440-452 nm), $^6H_{5/2} \rightarrow {}^4I_{13/2}$ (466 nm), $^6H_{5/2} \rightarrow {}^4I_{9/2}$ (480 nm).[23] They are more intense than the CTS band, which indicates that the emission process can be stimulated upon photoexcitation into the CTS band or directly into the f-f transitions of Sm^{3+}. The emission spectrum of **TBA-SmMo$_{16}$** (λ_{ex} = 286 nm) consists in characteristic emission peaks of the Sm^{3+} ion at 564 nm ($^4G_{5/2} \rightarrow {}^6H_{5/2}$), 599 and 607 nm ($^4G_{5/2} \rightarrow {}^6H_{7/2}$), 650 nm ($^4G_{5/2} \rightarrow {}^6H_{9/2}$), and 707 nm ($^4G_{5/2} \rightarrow {}^6H_{11/2}$).[23] Its emission color is more orange than for **TBA-EuMo$_{16}$** with CIE chromaticity coordinates of (0.5841, 0.4065) (Figure S11). The decay time of the $^4G_{5/2} \rightarrow {}^5H_{7/2}$ emission (λ_{exc} = 286 nm) is 0.28 ± 0.01 ms (Figure S12).

TBA-EuMo$_{16}$ and **TBA-SmMo$_{16}$** dissolved in acetonitrile exhibit an orange luminescence at room temperature (Figure S13). The PL spectrum of $[Sm(Mo_8O_{26})_2]^{5-}$ is similar to that of **TBA-SmMo$_{16}$**, confirming the robustness of the Sm-POM. The PL spectrum of $[Eu(Mo_8O_{26})_2]^{5-}$ in solution shows slight changes compared to that monitored in the solid state. In particular, the weakly intense $^5D_0 \rightarrow {}^7F_0$ transition (576 nm) is distinguishable. In addition, the $^5D_0 \rightarrow {}^7F_2/{}^5D_0 \rightarrow {}^7F_1$ intensity ratio is increased (0.64 *vs* 0.38 for **TBA-EuMo$_{16}$**). This indicates that the site symmetry of the Eu^{3+} ion decreases.[12] Nevertheless, as no change is detectable in the Raman spectrum (Figure S5), this symmetry reduction should be limited, and anyway much less pronounced than for **EuW$_{10}$** which shows a strong inversion of the $^5D_0 \rightarrow {}^7F_2/{}^5D_0 \rightarrow {}^7F_1$ intensity ratio in water.[8]

TPP-EuMo$_{16}$ has an intense orange-red solid-state emission at room temperature (Figure S14), with CIE chromaticity coordinates of (0.6281, 0.3666) very close to those of **TBA-EuMo$_{16}$**. Their PLE and PL spectra (Figure S15) are comparable excepted for the $^5D_0 \rightarrow {}^7F_2/{}^5D_0 \rightarrow {}^7F_1$ intensity ratio which is increased to 0.5 for **TPP-EuMo$_{16}$**. Upon photoexcitation at 286 nm, the decay time of the $^5D_0 \rightarrow {}^7F_1$ transition is 5.30 ± 0.03 ms (Figure S12), similarly as observed for its TBA-counterpart. This evidences that the substitution of flexible TBA cations by more rigid TPP ones does not significantly impact the high PL performances of $[Eu(Mo_8O_{26})_2]^{5-}$ in the solid state. In contrast, the orange emission of **TTP-SmMo$_{16}$**, which is characterized by CIE chromaticity coordinates of (0.5757, 0.4054), is more intense than that of **TBA-SmMo$_{16}$** (Figure S14), and the decay time of the $^4G_{5/2} \rightarrow {}^5H_{7/2}$ transition (λ_{exc} = 286 nm) reaches 0.66 ± 0.01 ms. This is consistent with the change in the PLE spectrum profile in which the CTS band has the same intensity than the f-f transitions of Sm^{3+} (Figure S16), suggesting a better POM-to-Sm^{3+} energy transfer.

In summary, the $[Ln(Mo_8O_{26})_2]^{5-}$ (Ln = Eu, Sm) complexes are new luminescent Ln-POMs both in solution and in the solid state. The nonsolvated TBA-$LnMo_{16}$ compounds have been well structurally characterized. They show a high thermal stability in air and an efficient emission at room temperature. Noticeably, the PL performances of **TBA-EuMo$_{16}$** are close to those of the **EuW$_{10}$** reference, owing to structural similarities between $[Eu(Mo_8O_{26})_2]^{5-}$ and $[Eu(W_5O_{18})_2]^{9-}$. This makes **TBA-EuMo$_{16}$** a promising alternative Ln-POM emitter which is furthermore easily soluble in polar non-aqueous solvents. Both FT-Raman and PL spectroscopies confirmed the integrity of the $[Ln(Mo_8O_{26})_2]^{5-}$ complexes in acetonitrile. The TPP-derivatives were obtained by a cation metathesis reaction. They are also thermally robust and efficient phosphors. To go further, this work evidences the possibility to design crystallized supramolecular assemblies by combining the luminescent $[Ln(Mo_8O_{26})_2]^{5-}$ units with photoactive organic cations, paving the way toward novel multifunctional optical hybrid systems.

ASSOCIATED CONTENT

Supporting Information

Experimental section, crystallographic data, IR and Raman spectra, ATG measurements, PXRD patterns, Absorption, PL and PLE spectra, CIE diagrams, luminescence decay curves and extracted lifetimes. This material is available free of charge via the Internet at http://pubs.acs.org.

AUTHOR INFORMATION

Corresponding Author

*E-mail: helene.brault@cnrs-imn.fr (H.B.)
*E-mail: remi.dessapt@cnrs-imn.fr (R.D.)

ORCID

Hélène Serier-Brault: 0000-0002-3300-1347
Rémi Dessapt: 0000-0002-2862-7767
Eric Faulques: 0000-0002-7761-8509

NOTES

The authors declare no competing financial interests.

ACKNOWLEDGMENT

This work was supported by the CNRS, the Université de Nantes, the Ministère de l'Enseignement Supérieur et de la Recherche, and the LUMOMAT project supported by the *Région des Pays de la Loire.*

REFERENCES

(1) (a) Zhao, J.-W.; Li, Y.-Z.; Chen, L.-J.; Yang, G.-Y. Research progress on polyoxometalate-based transition-metal–rare-earth heterometallic derived materials: synthetic strategies, structural overview and functional applications. *Chem. Commun.*, **2016**, *52*, 4418-4445. (b) Ma, X.; Yang, W.; Chen, L.; Zhao, J. Significant developments in rare-earth-containing polyoxometalate chemistry: synthetic strategies, structural diversities and correlative properties. *CrystEngComm.*, **2015**, *17*, 8175-8197. (c) Yamase, T. Photo- and Electrochromism of Polyoxometalates and Related Materials. *Chem. Rev.*, **1998**, *98*, 307-325.

(2) AlDamen, M. A.; Clemente-Juan, J. M.; Coronado, E.; Martí-Gastaldo, C.; Gaita-Ariño, A. Mononuclear Lanthanide Single-Molecule Magnets Based on Polyoxometalates. *J. Am. Chem. Soc.*, **2008**, *130*, 8874-8875.

(3) Boglio, C.; Lemière, G.; Hasenknopf, B.; Thorimbert S.; Lacôte E.; Malacria; M. Lanthanide complexes of the monovacant Dawson polyoxotungstate [alpha1-$P_2W_{17}O_{61}$]$^{10-}$ as selective and recoverable Lewis acid catalysts. *Angew. Chem. Int. Ed.*, **2006**, *45*, 3324-3327.

(4) (a) Kaczmarek, A. M.; Van Hecke, K.; Van Deun, R. Low-Percentage Ln^{3+} Doping in a Tetranuclear Lanthanum Polyoxometalate Assembled from $[Mo_7O_{24}]^{6-}$ Polyanions Yielding Visible and Near-Infrared Luminescence. *Inorg. Chem.*, **2017**, *56*, 3190-3200. (b) Ritchie, C.; Moore, E. G.; Speldrich, M.; Kögerler, P.; Boskovic, C. Terbium Polyoxometalate Organic Complexes: Correlation of Structure with Luminescence Properties. *Angew. Chem. Int. Ed.*, **2010**, *49*, 7702-7705. (c) Yamase, T. Polyoxometalates for Molecular Devices: Antitumor Activity and Luminescence. *Mol. Eng.*, **1993**, *3*, 241-262. (d) Wang, J.; Ma, P.; Li, S.; Xu, Q.; Li, Y.; Niu, J.; Wang, J. Polyoxotungstate Cluster Species Connected by Glutamic Acid and Europium. *Inorg. Chem.*, **2019**, 58, 57-60.

(5) Blasse, G.; Dirksen, G. J.; Zonnevijlle, F. The luminescence of some lanthanide decatungstates and other polytungstates, *J. Inorg. Nucl. Chem.*, **1981**, *43*, 2847-2853.

(6) Zhang, T.; Li, H.-W.; Wu, Y.; Wang, Y.; Wu, L. Self-Assembly of an Europium-Containing Polyoxometalate and the Arginine/Lysine-Rich Peptides from Human Papillomavirus Capsid Protein L1 in Forming Luminescence-Enhanced Hybrid Nanoparticles. *J. Phys. Chem. C*, **2015**, *119*, 8321-8328.

(7) Xia, C.; Wang, Z.; Sun, D.; Jiang, B.; Xin, X. Hierarchical Nanostructures Self-Assembled by Polyoxometalate and Alkylamine for Photocatalytic Degradation of Dye. *Langmuir*, **2017**, *33*, 13242-13251.

(8) Salomon, W.; Dolbecq, A.; Roch-Marchal, C.; Paille, G.; Dessapt, R.; Mialane, P.; Serier-Brault H. A multifunctional dual-luminescent polyoxometalate@metal-organic framework EuW_{10}@UiO-67 composite as chemical probe and temperature sensor. *Front. Chem.*, **2018**, *6*, 425.

(9) Wang, Z.; Zhang, R.; Ma, Y.; Peng, A.; Fua, H.; Yao, J. Chemically responsive luminescent switching in transparent flexible self-supporting $[EuW_{10}O_{36}]^{9-}$-agarose nanocomposite thin films. *J. Mater. Chem.*, **2010**, *20*, 271-277.

(10) Zhang, H.; Guo, L.; Xie, Z., Xin, X.; Sun, D.; Yuan, S. Tunable Aggregation-Induced Emission of Polyoxometalates via Amino Acid-Directed Self-Assembly and Their Application in Detecting Dopamine. *Langmuir*, **2016**, *32*, 13736-13745.

(11) Zhang, T.; Liu, S.; Kurth, D. G.; Faul, C. F. J. Organized Nanostructured Complexes of Polyoxometalates and Surfactants that Exhibit Photoluminescence and Electrochromism. *Adv. Funct. Mater.*, **2009**, *19*, 642-652.

(12) Yan, B.; Cuan, J. Co-assembly and luminescence tuning of hybrids with task-specified ionic liquid encapsulating and linking lanthanide-polyoxometalates and complexes. *Photochem. Photobiol. Sci.*, **2014**, *13*, 1469-1475.

(13) Shen, D.-F.; Li, S.; Liu, H.; Jiang, W.; Zhang Q.; Gao, G.-G. A durable and fast-responsive photochromic and switchable luminescent polyviologen–polyoxometalate hybrid. *J. Mater. Chem. C*, **2015**, *3*, 12090-12097.

(14) (a) Ballardini, R.; Chiorboli, E.; Balzani, V. Photophysical properties of $Eu(SiW_{11}O_{39})_2^{13-}$ and $Eu(BW_{11}O_{39})_2^{15-}$. *Inorg. Chim. Acta*, **1984**, *95*, 323-327. (b) Mialane, P.; Lisnard, L.; Mallard, A.; Marrot, J.; Antic-Fidancev, E.; Aschehoug, P.; Vivien, D.; Sécheresse, F. Solid-State and Solution Studies of $\{Ln_n(SiW_{11}O_{39})\}$ Polyoxoanions: An Example of Building Block Condensation Dependent on the Nature of the Rare Earth. *Inorg. Chem.*, **2003**, *42*, 2102-2108. (c) Zhang, H. Y.; Xu, L.; Wang, E. B.; Jiang, M.; Wu, A. G.; Li, Z. Photochromic behavior and luminescent properties of novel hybrid organic–inorganic film doped with Preyssler's heteropoly acid $H_{12}[EuP_5W_{30}O_{110}]$ and polyvinylpyrrolidone. *Mater. Lett.*, **2003**, 57, 1417-1422.

(15) Yamase, T.; Naruke, H.; Sasaki, Y. Crystallographic characterization of the polyoxotungstate $[Eu_3(H_2O)_3(SbW_9O_{33})(W_5O_{18})_3]^{18-}$ and energy transfer in its crystalline lattices. *J. Chem. Soc. Dalton Trans.*, **1990**, 1687-1696.

(16) Kitamura, A.; Ozeki, T.; Yagasaki, A. β-Octamolybdate as a Building Block. Synthesis and Structural Characterization of Rare Earth–Molybdate Adducts. *Inorg. Chem.*, **1997**, *36*, 4275-4279.

(17) Baldoví, J. J.; Duan, Y.; Bustos, C.; Cardona-Serra, S.; Gouzerh, P.; Villanneau, R.; Gontard, G.; Clemente-Juan, J. M.; Gaita-Ariño, A.; Giménez-Saiz, C.; Proust, A.; Coronado, E. A single ion magnets based on lanthanoid polyoxomolybdate complexes. *Dalton Trans.*, **2016**, *45*, 16653-16660.

(18) Abramczyk, H.; Paradowska-Moszkowska, K. The correlation between the phase transitions and vibrational properties by Raman spectroscopy: liquid-solid β and solid β-solid α acetonitrile transitions. *Chem. Phys.*, **2001**, *265*, 177-191.

(19) (a) Dong, K.; Ma, P.; Wu, H.; Wu, Y.; Niu, J.; Wang, J. Cobalt- and Nickel-Containing Germanotungstates Based on Open Wells–Dawson Structure: Synthesis and Characterization of Tetrameric Anion. *Inorg. Chem.*, **2019**, *58*, 6000-6007. (b) Ni, L.; Xu, H.; Li, H.; Zhao, H.; Diao, G. 3D-architecture via self-assembly of Krebs-type polyoxometalate $\{[Na_{10}(H_2O)_{26}][Sb_2W_{20}Zn_2O_{70}(H_2O)_6]\}$. *Polyhedron*, **2018**, *155*, 59-65.

(20) Blasse, G. Luminescence from the Eu^{3+} ion in D_{4d} Symmetry. *Inorg. Chim. Acta*, **1988**, *142*, 153-154.

(21) Yan, Y.; Li, B.; Li, W.; Li, H.; Wu, L. Controllable vesicular structure and reversal of a surfactant-encapsulated polyoxometalate complex. *Soft Matter.*, **2009**, 5, 4047-4053.

(22) (a) Wu, H.; Yan, B.; Li, H.; Singh, V.; Ma, P.; Niu, J.; Wang, J. Enhanced Photostability Luminescent Properties of Er^{3+}-Doped Near-White-Emitting $Dy_xEr_{(1-x)}$-POM Derivatives. *Inorg. Chem.*, **2018**, *57*, 7665-7675. (b) Artetxe, B.; Reinoso, S.; San Felices, L.; Gutiérrez-Zorrilla, J. M.; Garcia, J. A.; Haso, F.; Liu, T.; Vicent, C. Crown-Shaped Tungstogermanates as Solvent-Controlled Dual Systems in the Formation of Vesicle-Like Assemblies. *Chem. Eur. J.*, **2015**, *21*, 7736-7745.

(23) Kodaira, C. A.; Brito, H. F.; Teotonio, E. E. S.; Felinto, M. C. F. C.; Malta, C. A.; Brito, G. E. S. Photoluminescence behavior of the Sm^{3+} and Tb^{3+} ions doped into the $Gd_2(WO_4)_3$ matrix prepared by the Pechini and ceramic methods. *J. Braz. Chem. Soc.*, **2004**, *15*, 890-896.

For Table of Contents Only